Journal of Engineering Science and Technology
Vol. 11, No. 2 (2016) 212 - 227

MODELLING AND OPTIMISATION OF A BIMORPH PIEZOELECTRIC CANTILEVER BEAM IN AN ENERGY HARVESTING APPLICATION

CHUNG KET THEIN[1,*], BENG LEE OOI[2], JING-SHENG LIU[3], JAMES M. GILBERT[3]

[1]School of Engineering, Taylor's University, Taylor's Lakeside Campus, No. 1 Jalan Taylor's, 47500, Subang Jaya, Selangor DE, Malaysia
[2]Faculty of Integrative Sciences and Technology, Quest International University Perak, Plaza Teh Teng Seng (Level 2), 227, Jalan Permaisuri Bainun, 30250 Ipoh, Perak, Malaysia
[3]School of Engineering, University of Hull, HU6 7RX, Hull, UK
*Corresponding Author: ckthein@gmail.com

Abstract

Piezoelectric materials are excellent transducers in converting vibrational energy into electrical energy, and vibration-based piezoelectric generators are seen as an enabling technology for wireless sensor networks, especially in self-powered devices. This paper proposes an alternative method for predicting the power output of a bimorph cantilever beam using a finite element method for both static and dynamic frequency analyses. Experiments are performed to validate the model and the simulation results. In addition, a novel approach is presented for optimising the structure of the bimorph cantilever beam, by which the power output is maximised and the structural volume is minimised simultaneously. Finally, the results of the optimised design are presented and compared with other designs.

Keywords: Piezoelectric, Multi-disciplinary optimisation, Shape optimisation, Energy harvesting, Bimorph cantilever beam.

1. Introduction

Recent trends in electronic technology have enabled a decrease in both the size and power consumption of complex digital systems, meaning that wireless sensor networks are now poised to be a significant enabling technology in many fields. It

Nomenclatures

b^*	Strain related to vertical displacement of the beam
c	Damping coefficient
C_p	Capacitance of the piezoelectric device, F
d	Piezoelectric strain coefficient
k	Coupling coefficient
l_b	Length of base, mm
l_f	Length of clamp, mm
l_m	Length of tip mass, mm
m_{eff}	Effective mass, kg
m_{tip}	Tip mass, kg
t_c	Thickness of the piezoelectric material, mm
t_{sh}	Thickness of the shim material, mm
V_s	Structural volume, mm^3
Y	Young's modulus, GPa
Y_c	Young's Modulus for the piezoelectric material, GPa

Greek Symbols

ε	Vertical displacement at the tip end, m

is highly desirable for wireless sensor nodes to be self-powered. There are many potential power sources for wireless sensor nodes, especially ambient vibrations around the node [1, 2]. It is possible to convert part of the ambient energy around the node into electrical energy using various methods, including the use of piezoelectric beams. Piezoelectric materials are physically deformed in the presence of an electric field, and conversely, produce an electrical charge when deformed. When mechanical stress is applied to a piezoelectric material, an open-circuit voltage (a charge separation) appears across the material. Likewise, if a voltage is placed across the material, mechanical stress develops in the material. In this paper, a 31-mode piezoelectric material, mounted as a cantilever beam, is investigated and optimised. The 31-mode material is able to create relatively large deflections, takes up less space, and has lower resonant frequency than material used in 33-mode [3].

Many recent studies have focused on the performance of a cantilever beam with various geometries, in order to identify design geometries that maximise the scavenging performance in terms of output power density [4-6]. Sodano et al. [7, 8] performed experiments to investigate a piezoelectric composite actuator for power generation. Three different materials were assessed for their effectiveness in power-harvesting applications: Quick Pack, piezoelectric material (PZT) (lead zirconate titanate), and MFC (micro-fibre composite) were mounted to a cantilever beam which was tested at 12 different resonant frequencies. PZT was shown to be more effective in the random vibration environments that are usually encountered when dealing with ambient vibrations.

Miller et al. [9] reported an increase in the weighted strain of a cantilever with the addition of a slit through the middle of the beam, which yielded a weighted strain that is more than twice that of a rectangular cantilever. Hence, the authors concluded that a typical solid rectangular cantilever beam is non-optimized for micro-scale energy scavenging. Mateu and Moll [10] performed an analytical comparison between rectangular and triangular cantilevers in which they assumed

uniform stress across the width of the cantilever. This revealed that a triangular cantilever with the same beam volume as a rectangular beam has a higher average strain and larger deflection for a given load, thereby producing more power per unit volume. Simon and Yves [11] showed that the tapered beam with 0.3° slope angle could increase the energy harvested by 69%. These proved that the geometry of the cantilever beam affects the power output. Roundy also reported that the power density of a beam can be increased by using a smaller volume, and that the strain is distributed more evenly in the case of a trapezoidal cantilever beam, which generates more than twice the energy of a rectangular beam for a given volume [12]. Dhakar et al. [13] demonstrated that by reducing the resonant frequency of the trapezoidal cantilever beam the overall power output could significantly be increased. All the above mentioned studies suggest that optimising the structural details of the trapezoidal cantilever beam may further increase the power output.

The power output of a cantilever beam is directly related to the shape. What is the best design of a trapezoidal cantilever beam that generates the maximum power density? To answer this question, the sensitivity of power density to beam should be examined. In this paper, a multi-objective method, MOST (multifactor optimisation of structures technique) [14-15], is extended to automatically accommodate and execute problems related to energy-harvesting optimisation. The MOST technique utilizes commercially available finite element codes (e.g., ANSYS) and combines static analysis, dynamics analysis (for vibration frequency), and a unique optimisation technique, with the aim of simultaneously increasing both the power output and the power density. The MOST optimisation system can efficiently and systematically solve complex engineering-design problems, which may have multiple objectives and involve multiple disciplines, by performing a parameter profile analysis [16], thereby seeking the optimum solution. This method incorporates an assessment system which brings the scores and merit indices into a defined range (in this case 0–10) for all performance and loading cases. These features make MOST a powerful, cost-effective, and reliable tool with which to optimise complex structural systems.

This paper proposes an alternative method of predicting the power output of a piezoelectric cantilever beam by static and dynamic (modal) analyses using the finite element method. The power outputs of the proposed method are verified by comparison with the results of both experimental and analytical analyses (the Roundy method [3]). A new method is presented in optimising a bimorph piezoelectric cantilever beam in an energy harvesting application, with the aim of simultaneously maximising power output and minimising structural volume, while also satisfying the strength and stiffness requirements of the structure. The performance of the optimised design is compared with triangular and rectangular shapes.

2. Predicting the output power of piezoelectric generator designs with different geometrical shapes using finite element analysis (FEA)

The constitutive equations for a piezoelectric material are as follows [17]:

$$\delta = \sigma/_{Y} + dE$$
$$D = \varepsilon E + d\sigma \quad (1)$$

where δ is mechanical strain, σ is mechanical stress, Y is the modulus of elasticity, d is the piezoelectric strain coefficient, E is the electric field, D is electric displacement, and ε is the dielectric constant of the piezoelectric material. Roundy [3] proposed that the magnitude of voltage transferred to the load for a piezoelectric bender can be given as follows (assuming that the driving frequency is not matched with the natural frequency):

$$V = \frac{-j\omega \dfrac{Y_c d t_c b^*}{\varepsilon}}{\left[\dfrac{1}{RC_p}\omega_n^2 - \left(\dfrac{1}{RC_p} + 2\zeta\omega_n\right)\omega^2\right] + j\omega\left[\omega_n^2\left(1+k^2\right) + \dfrac{2\zeta\omega_n}{RC_p} - \omega^2\right]} A_{in}^2 \qquad (2)$$

where V is the generated voltage from the piezoelectric material, ω is the driving frequency, Y_c is Young's Modulus for a piezoelectric material, d is the piezoelectric strain coefficient, t_c is the thickness of the piezoelectric material, b^* is strain related to vertical displacement of the beam, ε is the dielectric constant of the piezoelectric material, R is the load resistance, C_p is the capacitance of the piezoelectric device, ω_n is the natural frequency of the system, ζ is the mechanical damping ratio, k is a coupling coefficient, and A_{in} is the magnitude of the input acceleration.

This section focuses on the development of the power equation of a piezoelectric bender. Several terms from Eq. (2) need to be redefined to accommodate the results of the FEA. Figure 1 shows a schematic of a piezoelectric bender.

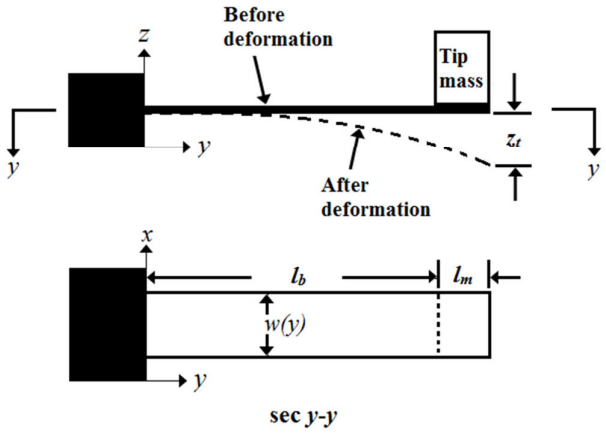

Fig. 1. Schematic piezoelectric bender.

In Fig. 1, l_b is the length of the base, l_m is the length of the tip mass, z_t is the vertical deflection of the cantilever beam tip, and $w(y)$ is the width of the piezoelectric material in terms of the electrode length (l_e). First, the mechanical damping ratio of the system can be stated as:

$$\zeta = \frac{c}{2m_{eff}\omega_n} \qquad (3)$$

where m_{eff} is the effective mass and c is a damping coefficient. The effective mass and natural frequency can be found from the FEA. Second, the capacitance of the beam is defined as:

$$C_p = \int_0^{l_e} \frac{n_c \varepsilon w(y)}{t_c} dx \tag{4}$$

where n_c is the number of piezoelectric layers. Using Hooke's law, b^* in Eq. (2) can be related to the average element stress (σ_{ave}) as follows:

$$\sigma_{ave} = \frac{1}{n_c} \sum_{c=1}^{n_c} \sigma_c \tag{5}$$

$$b^* = \frac{\sigma_{ave}}{Y_c z_t} \tag{6}$$

The power transferred to the load is simply V^2/R. Equation (2) can be further simplified if the natural frequency (ω_n) is assumed that it is equivalent to the driving frequency (ω). This is because the generated power is maximised when the vibration frequency is equal to the resonant frequency. Thus, the natural frequency and the environment frequency must be very similar [3, 18]. The power output (P) of the beam can then be formulated as follows:

$$P = \frac{1}{2\omega_n^2} \frac{RC_p^2 \left(\frac{dt_c \sigma_{ave}}{\varepsilon z_t} \right)^2}{\left(4\zeta^2 + k^4\right)\left(RC_p\omega_n\right)^2 + 4\zeta k^2 \left(RC_p\omega_n\right) + \left(2\zeta\right)^2} A_{in}^2 \tag{7}$$

The optimum resistance can be found by differentiating Eq. (7) with respect to R, setting the result equal to zero and solving for R. The optimum resistance (R_o) is as follows:

$$R_o = \frac{2\zeta}{\omega_n C_p \sqrt{4\zeta^2 + k^4}} \tag{8}$$

3. Verification of ANSYS Simulations, Experimental and Theoretical Results

3.1. Design constraints, load, and ANSYS simulation setup

A cantilever beam is modelled and analysed. The ANSYS SOLID92 element is used to generate the model rather than the SOLID98 element, although both elements are 10-node tetrahedral shapes suitable for large deflection and stress-stiffening behaviour. The SOLID92 element adapts well to the free meshing of irregular shapes. Both static analysis and dynamic (modal) analysis (for vibration frequency) are performed in the analysis. The cantilever beam (known as a 'bimorph' system) is composed of two layers of piezoelectric materials and a layer of shim material. The initial model consists of 9620 elements (both piezoelectric and shim elements) with a uniform element length of 0.8 mm. Figure 2 shows a schematic diagram of the design domains, geometric constraints,

load, and boundary conditions of the design. Points *A* and *D* are fixed at three coordinates (*x*, *y*, and *z*). A concentrated pressure is applied at the free end of the cantilever beam (between *B* and *C*). The initial dimensions of the beam are listed in Table 1. The values of the mechanical and electric properties of the piezoelectric material (PZT-5A4E) and brass shim are given in Table 2 [19, 20].

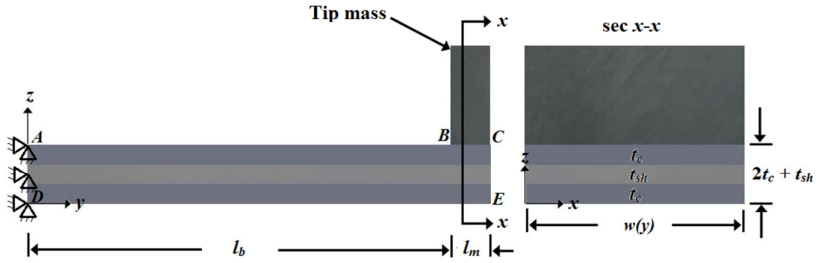

Fig. 2. Load and boundary conditions of the simulation setup.

Table 1. Dimensions of the initial design.

Parameters	Initial value (mm)
Thickness of piezoelectric material (t_c)	0.19
Thickness of shim material (t_{sh})	0.13
Length of base (l_b)	21.5
Length of tip mass (l_m)	2.00
Effective length of piezoelectric material PZT ($l_e = l_m + l_b$)	23.5
Width (w(y)) $1 \leq w(y) \leq 12.7$ mm	12.7

Table 2. Mechanical and electrical properties used in the FEA.

Property	Piezoelectric material	Brass shim
Young's modulus (GPa)	66	117
Yield stress (MPa)	24*	200
Maximum deflection (μm)	300	-
Poisson's ratio	0.31	0.324
Density (kg/m^3)	7800	7165
Relative dielectric constant	1800	-
d31 (m/V)	-190×10^{-12}	-

*Dynamic peak tensile strength [21]

3.2. Experiment setup

An experimental validation of the model based on Eq. (2) for a rectangular cantilever beam has been conducted. A vertical vibration generated from a shaker (model Number LDS-V406/8) was used to excite the cantilever and the vibration was also monitored using an accelerometer (MTN1800. The voltage generated by the piezoelectric material for a given load resistance was captured by an oscilloscope (Agilent MSO-6054A), along with the accelerometer signal). The vibration is in the periodic behaviour [22]. The obtained data from the oscilloscope were transferred to the MATLAB workspace via a USB flash drive. In the

MATLAB workspace, the data were subjected to a fast Fourier transform, and the frequency spectrum of the generated voltage and the vibration source plotted.

The piezoelectric cantilever (PZT-5A4E) has effective dimensions of 23.5×12.7×0.51 mm with a tip mass of 4.1 g (Fig. 3). Because the tip mass is located off-centre at the free end of the cantilever beam, it introduces a torque and force which cause the material to bend. The structure is excited by a sinusoidal wave with an acceleration magnitude of 4.905 ms^{-2} in the frequency range of 50-90 Hz. The mechanical and electric properties of the piezoelectric and shim materials are given in Table 2.

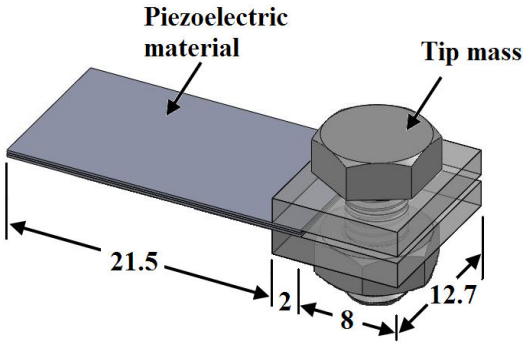

Fig. 3. Schematic diagram of the experiment setup (units in mm).

3.3. Verification of Experimental, Theoretical, and ANSYS Simulation Results

Figure 4 compares 14 sets of data (k = 1, 2, 3,...,14). All the experimental results show a resonant frequency (f_{re}) at around 73 Hz [23]; however, for clarity of presentation, they are separated by an offset frequency (f_{off} = 10 Hz) in order to plot them on a single graph. Hence the resistance-offset frequencies (f_k) on the horizontal axis for each set of data can be expressed as follows:

$$f_k = f_{re} + f_{off} \times k \tag{9}$$

In this research, the main aim is to maximise the power output, which is calculated by using Eq. (7). However, this equation must be verified before proceeding with the analysis. Therefore, a comparison is made between the existing technique (the Roundy method [3]), experimental results, and the proposed technique. Under the same setup in each case, but varying the resistance, Eq. (2) is calculated and plotted in Fig. 4 ("theory"). To calculate the power output using the proposed method, a finite element model of the rectangular piezoelectric cantilever beam was developed for use in predicting the behaviour of the beam under a concentrated load at the free end, as shown in Fig. 2. The average element stress and the vertical deflection are obtained in the analysis. The obtained values are substituted into Eq. (7) and the results are plotted in Fig. 4 as "ANSYS simulation".

The maximum power is produced when the resistance is in the range 30–65 kΩ (Fig. 4). The results of the ANSYS simulation and the theoretical calculation

differ by approximately 4.29%, whereas the experiment results are markedly different from these two sets of results. Many factors that may affect the experiment result, including the surrounding environment, the position of the tip mass, and the sensitivity of the apparatus. Hence, the error in the experiment is about 13% – 45% compared with the FEA. However, the frequency response for each load resistance and the effect of the load do show similar trends to both theory and simulation. Table 3 shows that the percentage of discrepancy of resistance-offset frequency.

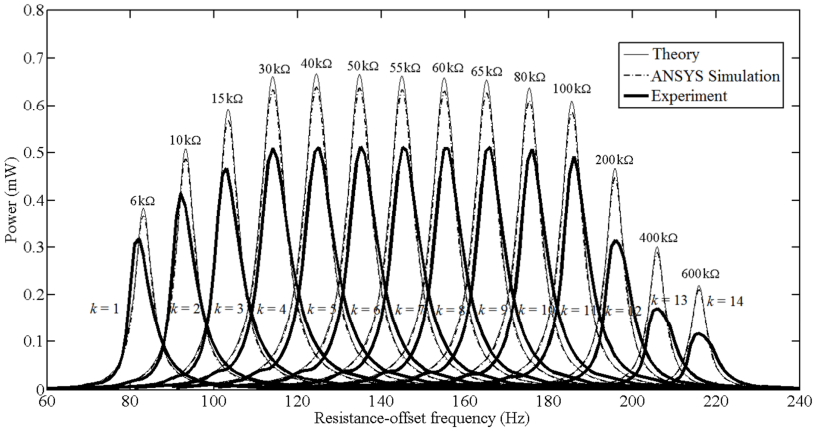

Fig. 4. Comparison of theoretical calculations, ANSYS simulation, and experimental results for output power.

Table 3. Percentage of discrepancy of theory, experiment and ANSYS simulation.

Resistance (kΩ)	Percentage discrepancy		
	Theoretical and Experiment	ANSYS simulation and Experiment	ANSYS simulation and Theoretical
6	16.78	13.06	4.29
10	17.91	14.23	
15	20.71	17.17	
30	22.68	19.22	
40	23.10	19.66	
50	22.69	19.23	
55	22.54	19.07	
60	22.52	19.06	
65	21.59	18.09	
80	20.22	16.65	
100	18.87	15.24	
200	32.20	29.17	
400	43.08	40.54	
600	46.85	44.47	

3.4. Optimisation methodology – multifactor optimisation of structures technique

The requirements for a complex structural design dictate that the optimisation must involve multiple objectives, multiple disciplines, and a large number of design variables. An $m \times n$ matrix (d_{ij})—the so-called performance data matrix (PDM)—is defined by a set of performance parameters P_i (i = 1, 2,…, m) and loading case parameters C_j (j = 1, 2,…, n), respectively. The PDM is a schematic representation of a collection of data as shown in Table 4. Thus, the data point d_{ij} is the i-th performance P_i of the structure at the loading case C_j. In this case the data points of the matrix are obtained by a finite element analysis of the structure. The matrix lists every loading case as well as every performance parameter relevant to the individual loading cases.

Table 4. Performance data matrix.

	C_1	C_2	⋯	C_n
P_1	d_{11}	d_{12}	⋯	d_{1n}
P_2	d_{21}	d_{22}	⋯	d_{2n}
⋮	⋮	⋮		⋮
P_m	d_{m1}	d_{m2}	⋯	d_{mn}

A parameter profile matrix (PPM) is created to review the profile of the performances for different loading cases (Table 5). To simplify the calculations, the values of the performance indices are normalised to the range 0–10. This enables different loading cases and parameters to be compared, in order to gain an overall perspective of the characteristics of the system. The PPM assesses the character of the structure with respect to the actual performances at their worst acceptable limits and the best expected values of the performances.

Table 5. Parameter profile matrix.

	C_1	C_2	⋯	C_n
P_1	D_{11}	D_{12}	⋯	D_{1n}
P_2	D_{21}	D_{22}	⋯	D_{2n}
⋮	⋮	⋮		⋮
P_m	D_{m1}	D_{m2}	⋯	D_{mn}

The data point D_{ij} for one acceptable limit (e.g., lower limit) is calculated as follows:

$$D_{ij} = \frac{d_{ij} - l_{ij}}{b_{ij} - l_{ij}} \times 10 \tag{10}$$

where d_{ij} is the actual value of the performance obtained from the PDM, and l_{ij} and b_{ij} are the lower acceptable limit and the best expected value, respectively. Eq. (10) is valid for $l_{ij} < d_{ij} < b_{ij}$; for $d_{ij} > b_{ij}$, $D_{ij} = 10$; and for $d_{ij} < l_{ij}$, $D_{ij} = 0$. The

data point for the cases of acceptable upper limit and double acceptable limits can be calculated in a similar way.

The mean and standard deviation (SD) are calculated for each parameter and loading case in each column and row in the PPM. A well-designed system should have low SDs and high mean values (close to 10). The existence of high SDs signifies that the system is likely to have significant problematic areas. Therefore, a high SD for a row indicates variable system performance at different loading cases for a particular parameter. Conversely, a high SD for a column indicates the system is likely to have significant problematic performance for the specific loading case.

The system can be further analysed using a parameter performance index (PPI) and a case performance index (CPI), which are defined as follows:

$$PPI_i = \frac{n}{\sum_{j=1}^{n} 1/D_{ij}} \quad , \quad i = 1, 2, \cdots, m \quad \text{and}$$

$$CPI_j = \frac{m}{\sum_{i=1}^{m} 1/D_{ij}} \qquad j = 1, 2, \cdots, n \tag{11}$$

When i-th parameter is very vulnerable, some data points D_{ij} of the PPM will have values close to 0 and hence the PPI_i will also close to 0. Similarly, when the system is vulnerable at the j-th loading case, CPI_j will be close to 0. The highest values for PPI and CPI are 10. PPI and CPI values close to 10 indicate good design, whereas values close to zero indicate poor design. The mean values, CPIs, PPIs, and SDs provide an overall performance assessment for the system and loading cases. These indices are calculated by summing the inverse of the data points as a performance rating to avoid the effect associated with low scores being hidden by high scores. The mean values are not used directly to rate the performance. The system may be reviewed by using the information in the indices, as follows:

- A comparison of PPIs indicates whether the system performs better with respect to some performances than to others.
- A comparison of CPIs shows whether the system performs better under certain loading cases than under others.

According to the matrix profile analysis, PPI and CPI are measures of the vulnerability of each performance parameter and each loading case, respectively. Hence, the integration of PPI and CPI indicates the vulnerability of a particular parameter/loading case combination. An overall performance index (OPI) is used to develop the overall objective function. The OPI, which takes the form of a qualitative score, can be established for the system by considering all the performances and all the loading cases. The OPI function lies in the range of 0–100. The OPI can be expressed as follows:

$$OPI = \frac{100}{m \times n} \sum_{i=1}^{m} \sum_{j=1}^{n} W_{P_i} \cdot PPI_i \times W_{C_j} \cdot CPI_j \tag{12}$$

where W_{P_i} and W_{C_j} are weighting factors in the range of 0–1 reflecting the preference for each performance parameter and each loading case. The OPI can be used to compare the performances of different designs. The higher the OPI

score, the more reliable the design would be. The objective function is maximised using the effective zero-order method, employing conjugate search directions [13]. An effective polynomial interpolation uni-dimensional search method is also used in the algorithm. This optimisation technique has the advantage of forcing the performances to approach their optimal values. The nearer the performances to the acceptable limits, the stricter the 'punishment' (penalties) will be.

4. Electrical Energy and Structural Optimisation of a Bimorph Piezoelectric Cantilever Beam

The power output of a cantilever beam is directly related to its shape. This study considers the sensitivity of the power to the shape of the cantilever. The main objective is to find the optimum geometrical shape of a bimorph cantilever beam that yields the maximum power and has the minimum structural volume. In addition, the beam must satisfy the strength and stiffness requirements. A dynamic analysis (for the vibration frequency) is also required in the power calculation as indicated in Eq. (7).

4.1. Formulation of the optimisation problem

In this study, the optimal shape of the bimorph cantilever is determined by MOST, which is used in conjunction with the ANSYS finite element software. The design problem is therefore to maximise the power output and the average element stress, and simultaneously to minimise the structural volume, subject to the design constraints. The optimisation to be solved is stated as follows:

$$
\begin{aligned}
&\text{find} && X = (x_1, x_2, \ldots, x_k)\\
&\min && \{V_s(X)\}\\
&\quad \text{and}\\
&\max && \{P_j(X) \text{ and } \sigma_{\text{ave},j}(X)\}\\
&\text{s.t.} && \{P_j \geq P_{\text{ini},j};\ V_s \leq V_{s,\text{ini}};\ \sigma_{\text{ave},j} \geq \sigma_{\text{ini},j};\ \sigma_{\max,j} \leq \sigma_y;\ \delta_{\text{ini},j} \leq \delta_j \leq \delta_{\text{lim},j}\} \text{ and}\\
&&& \{x_i^{\min} \leq x_i \leq x_i^{\max},\ i = 1,2,\ldots,k\}\\
&&& j = 1, 2, \ldots, n
\end{aligned}
$$

where k is the number of design variables, V_s is the structural volume (excluding the volume of the tip mass), σ_{ave} is the average element stress of the structure, δ is the displacement of point E (see Fig. 2), $\sigma_{\max}$ is the maximum Von Mises stress of the structure, and P is the power output. The subscript 'ini' indicates the initial value for the structure (here, the initial iteration when $n_i = 0$), and n is the number of loading cases (here, $n = 1$). The subscript 'lim' indicates a specified performance limit for the structure. In this research, the cantilever beam is optimised to carry a tip mass of 4.1 g with a maximum vertical displacement of $\delta_{\text{lim}} = 300$ μm at any node, satisfying a maximum strength of $\sigma_y = 24$ MPa (see Table 1). $x_i^{\min}$ and $x_i^{\max}$ are the lower and upper bounds of the design variables of x_i, respectively. There are eight design variables in the structural model, which represent the width of the cantilever beam. In this case, the lower and upper bounds are set to 1 and 15 mm, respectively.

4.2. Optimisation results

The shape optimisation of the cantilever beam required n_i = 27 iterations to converge, as shown in Figs. 5 and 6, which depicts the evolution of the structural volume, the power output and the power density. A sharp increase in the output power is seen up to n_i = 5, because the width at the free end of the beam (where the tip mass is located) is reduced to a tenth of its original size. This is followed by a sharp decrease in power output up to n_i = 8, due to the removal of material from the structure and changing values of the natural frequency, damping ratio, resistance, and capacitance. Subsequently, the power output fluctuates before converging to an optimal solution at n_i = 27. The opposite trend is observed for the structural volume. The distribution of Von Mises stress for the initial and optimised designs is shown in Fig. 7. The tip mass is not shown in Fig. 7 but is followed the ANSYS simulation setup as shown in Fig. 2. The attributes of the initial and optimised designs are given in Table 6.

The resonant frequency of the initial and optimised designs are 113 Hz and 92 Hz respectively, as obtained from the FEA. The frequency is affected by the position and geometry (i.e., same volume but different shape) of the tip mass. More specifically, the natural frequency of the cantilever beam is affected by the height of the tip mass. Thus, appropriate dimensions should be chosen to suit the vibration design. In this case, the finite element models and the experiments models are similar except for the shape of the tip mass (see Figs. 2 and 4, respectively)

Roundy [12] reported that a triangular beam produces more than twice the power density of a rectangular beam. Table 7 lists the power density (per unit volume of piezoelectric material) and the dimensions of a rectangular beam, triangular beam, and the optimised shape of the present study (Fig. 8). Under the same constraints (i.e., the width of the free end is the same for both optimised design and triangular shape), the power density of the optimised design is superior to that of the triangular and rectangular shapes.

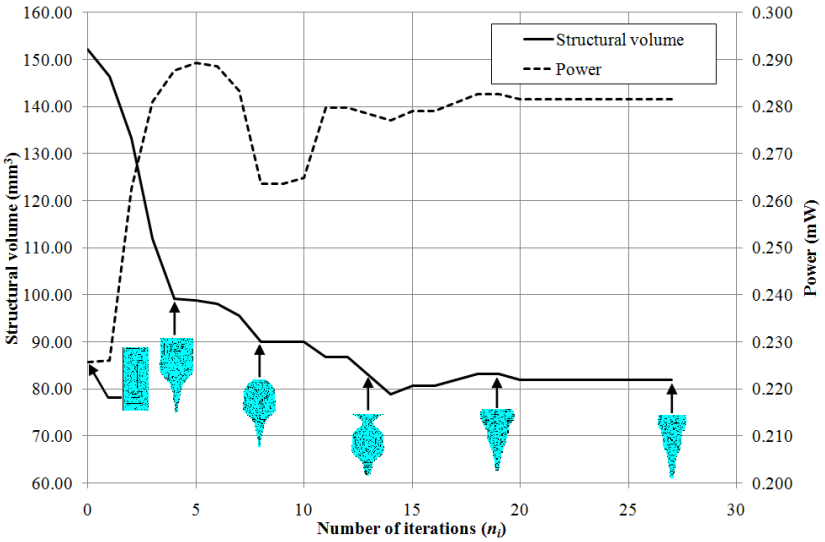

Fig. 5. Optimisation convergence history of the structural volume and power.

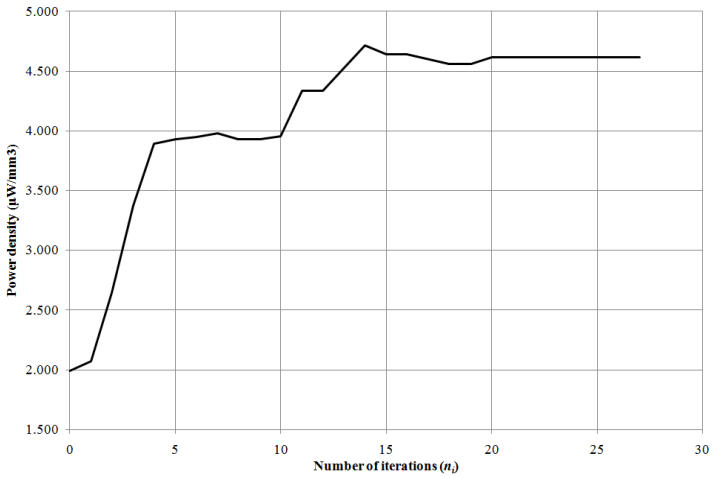

Fig. 6. Optimisation convergence history of the power density.

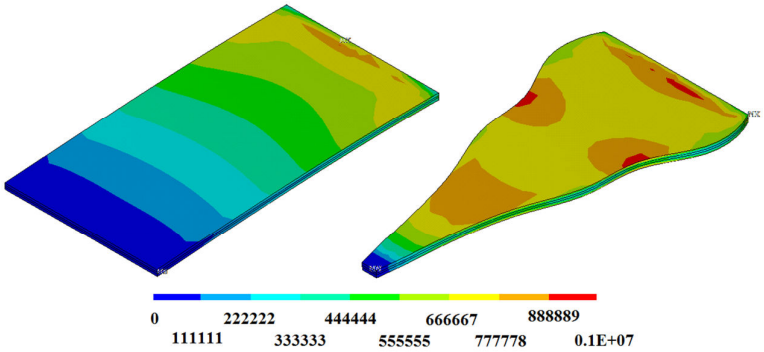

Fig. 7. Distribution of Von Mises stress for the initial design (left) and the optimised design (right) (Pa).

Table 6. Design attributes of the initial and optimised designs of a cantilever beam.

	Initial design	Optimised design
Power (mW)	0.226	0.282
Volume of piezoelectric material (mm^3)	113.41	60.97
Volume of shim material (mm^3)	38.80	20.86
Power density (µW/ mm^3)*	1.99	4.62
Maximum Von Mises stress (MPa)	0.89	1.00
Average element stress (MPa)	0.24	0.46
Maximum vertical displacement (µm)	8.48	12.50
Capacitance (nF)	50.07	26.92
Frequency (Hz)	113	92

*per unit volume of piezoelectric material

Table 7. Comparison of power density among beams with different shapes.

	Rectangular shape	Triangular shape	Optimised design
Volume of piezoelectric material (mm^3)	113.41	61.30	60.97
Power density ($\mu W/mm^3$)	1.99	4.49	4.62

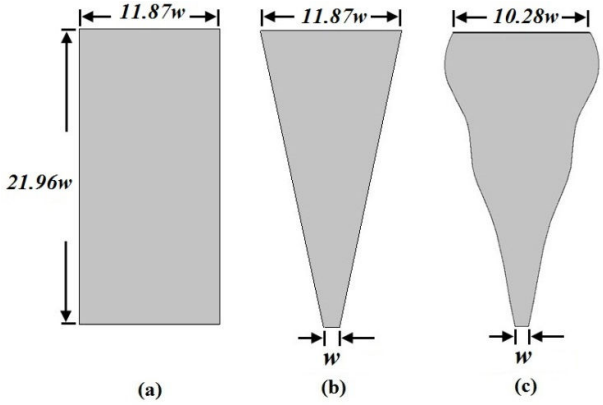

Fig. 8. Dimension of (a) rectangular, (b) triangular, and (c) optimised shapes (in ratio).

5. Conclusions

The output power is increased from approximately 0.226 to 0.282 mW, which corresponds to an increase of approximately 25% compared with the initial design. The structural volume (piezoelectric and shim material combined) is reduced significantly from 152.21 to 81.83 mm^3, representing a 46.2% saving in materials. The power density of the optimised design is more than twice that of the initial design, and the vertical deflection of the cantilever beam is increased by about 47%, from 8.48 to 12.50 μm. The maximum Von Mises stress shows an increase from 0.89 to 1.00 MPa. These results are well within the stiffness and strength constraints (δ_{lim} = 300 μm) and yield stress (σ_y = 24 MPa).

The results show good agreement between the finite element simulation and the theoretical results, which differs by approximately 4.5% in terms of the maximum power output. The maximum power output differs by ~20% between the finite element results and the experimental results, reflecting the fact that the experimental results were affected by various conditions (e.g., the environment effect). Therefore, the finite element simulation yields more accurate and reliable results compared with theoretical values. Thus, Eq. (7) presented in this paper is a novel development in estimating the power output of piezoelectric cantilever beams of various sizes and shapes by means of finite element analysis.

In the second part of this paper, a shape optimisation of the piezoelectric cantilever beam was presented. Simulation results indicate that the optimised design can generate 4.62 $\mu W/mm^3$ for a piezoelectric volume of 60.97 mm^3.

Future research will focus on maximising the power density by seeking the optimum "topology" of a bimorph cantilever beam. The results demonstrate the efficiency of the MOST technique.

The results obtained for the bimorph cantilever beam demonstrate that the proposed method was successful in identifying the optimum design, resulting in improved performance in terms of power output and power density.

In future work, the effect of stochastic forcing case on the optimised geometry may be considered.

References

1. Gilbert, J.M.; and Balouchi, F. (2008). Comparison of energy harvesting systems for wireless sensor networks. *International Journal of Automation and Computing*, 5(4), 334-347.
2. Roundy, S.; Steingart, D.; Frechette, L.; Wright, P.; and Rabaey. J. (2004). Power source for wireless sensor networks. *Wireless sensor network-Lecture Notes in Computer Science*, Springer-Verlag, 2920, 1-17.
3. Roundy, S. (2003). *Energy Scavenging for wireless sensor nodes with a focus on vibration to electricity conversion*. PhD thesis, University of California Berkely.
4. Goldschmidtboeing, F.; and Woias, P. (2008). Characterization of different beam shapes for piezoelectric energy harvesting. *Journal of Micromechanics and Microengineering*, 18(10), 1-7.
5. Benasciutti, D.; Moro, L.; and Zelenika, S. (2010). Vibration energy scavenging via piezoelectric bimorphs of optimized shapes. *Microsystem Technologies*, 16(5), 657-668.
6. Dietl, J.M.; and Garcia, E. (2010). Beam shape optimisation for power harvesting. *Journal of Intelligent Material Systems and Structures*, 21(6), 633-646.
7. Sodano, H.A.; Inman, D.J.; and Park, G. (2005). Comparison of Piezoelectric Energy Harvesting Devices for Recharging Batteries. *Journal of Intelligent Material Systems and Structures*, 16(10), 799-807.
8. Sodano, H.A.; Inman, D.J.; and Park, G. (2005). Generation and Storage of Electricity from Power Harvesting Devices. *Journal of Intelligent Material Systems and Structures*, 16(1), 67-75.
9. Miller, L.M.; Emley, N.C.; Shafer, P.; and Wright, P.K. (2008). Strain Enhancement within Cantilevered, Piezoelectric MEMS Vibrational Energy Scavenging Devices. *Advances in Science and Technology*, *Smart Materials and Mico/Nanosystems*, 54, 405-410.
10. Mateu, L.; and Moll, F. (2005). Optimum piezoelectric bending beam structures for energy harvesting using shoe inserts. *Journal of Intelligent Material Systems Structures*, 16, 835–845.
11. Simon, P.; and Yves, S.A. (2009). Electromechanical Performances of Different Shapes of Piezoelectric Energy Harvesters. *International Workshop Smart Materials and Structures*, 22-23 Oct 2009, Montreal, Canada

12. Roundy, S. (2005). On the effectiveness of vibration-based energy harvesting. *Journal of Intelligent Material Systems Structures,* 16, 809-823.
13. Dhakar, L.; Liu, H.; Tay, F.E.H.; and Lee, C. (2013). A new energy harvester design for high power output at low frequencies. *Sensors and Actuators*, 199, 344-352.
14. Liu, J.S.; and Hollaway, L. (2000). Design optimisation of composite panel structures with stiffening ribs under multiple loading cases. *Computers and Structures*, 78(4), 637-647.
15. Liu, J.S.; and Lu, T.J. (2004). Multi-objective and multi-loading optimization of ultralight weight truss materials. *International Journal of Solids and Structures*, 41, 619-635.
16. Liu, J.S.; and Thompson, G. (1996). The multi-factor design evaluation of antenna structures by parameters profile analysis. *Proceedings of the Instituition of Mechanical Engineers, Part B: Journal of Engineering Manufacture*, 210(5), 449-456.
17. Ikeda, T. (1996). *Fundamentals of piezoelectricity*. Oxford science publications, Oxford.
18. Shu, Y.C.; and Lien, I.C. (2006). Analysis of power output for piezoelectric energy harvesting systems. *Smart Materials and Structures*, 15, 1499-1512.
19. Gallas, Q.; Wang. G.; Papila, M.; Sheplak, M.; and Cattafesta, L. (2003). Optimization of synthetic jet actuators. *41st AIAA Aerospace Sciences Meeting and Exhibit,* Reno, NV, USA, AIAA-2003-0635.
20. Piezo System (2009), Inc. CATALOG #7C (2008). Retrieved July 31, 2009, from http://www.piezo.com/catalog.html.
21. Bert, C.W.; and Birman, V. (1998). Effects of stress and electric field on the coefficients of piezoelectric materials: one-dimensional formulation. *Mechanics Research Communications*, 25(2), 165-169.
22. Friswell, M.I.; Ali, S.F.; Bilgen, O.; Adhikari, S.; Lees, A.W.; and Litak, G. (2012). Non-linear piezoelectric vibration energy harvesting from a vertical cantilever beam with tip mass. *Journal of Intelligent Material Systems and Structures,* 23(13), 1505-1521.
23. Ooi, B.L. (2010). *Optimisation and frequency tuning concepts for a vibration energy harvester*. PhD Thesis, University of Hull.